ACS APPLIED MATERIALS & INTERFACES

Research Article

www.acsami.org

# Selective Targeting Capability Acquired with a Protein Corona Adsorbed on the Surface of 1,2-Dioleoyl-3-trimethylammonium Propane/DNA Nanoparticles

Giulio Caracciolo,*[,†,#] Francesco Cardarelli,[‡,#] Daniela Pozzi,[†] Fabrizio Salomone,[‡,§] Giuseppe Maccari,[‡] Giuseppe Bardi,[‡] Anna Laura Capriotti,[∥] Chiara Cavaliere,[∥] Massimiliano Papi,[⊥] and Aldo Laganà[∥]

[†]Department of Molecular Medicine, "Sapienza" University of Rome, Viale Regina Elena 291, 00161 Rome, Italy

[‡]Center for Nanotechnology Innovation @NEST, Istituto Italiano di Tecnologia, Piazza San Silvestro 12, 56127 Pisa, Italy

[§]NEST, Scuola Normale Superiore and Istituto Nanoscienze-CNR, Piazza San Silvestro 12, 56127 Pisa, Italy

[∥]Department of Chemistry, "Sapienza" University of Rome, P.le Aldo Moro 5, 00185 Rome, Italy

[⊥]Istituto di Fisica, Catholic University School of Medicine, Largo F. Vito 1, 00168 Rome, Italy

Supporting Information

**ABSTRACT:** A possible turning point in drug delivery has been recently reached: the protein shell, which covers nanocarriers in vivo, can be used for targeting. Here, we show that nanoparticles can acquire a selective targeting capability with a protein corona adsorbed on the surface. We demonstrate that lipid particles made of 1,2-dioleoyl-3-trimethylammonium propane (DOTAP) and DNA, upon interaction with human plasma components, spontaneously become coated with vitronectin that promotes efficient uptake in cancer cells expressing high levels of the vitronectin $\alpha_v\beta_3$ integrin receptor.

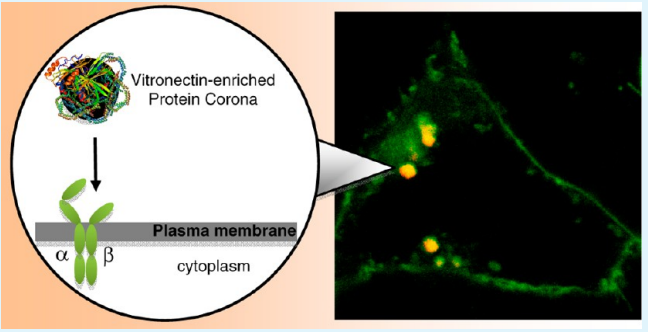


**KEYWORDS:** *targeting, drug delivery, nanoparticle, protein corona, cationic lipids*

## INTRODUCTION

Targeted drug delivery is being actively researched as a means to prolong, localize, and protect the interaction of drugs with target tissues. The main advantages of this approach are the diminution of the doses needed for therapeutic effect, the decrease of drug side effects, or adverse drug reactions and the reduced fluctuation in the levels of circulating drugs.[1−3] Active targeting requires the surface functionalization of a nanocarrier (NC) with monoclonal antibodies (mAbs), proteins, or small biomolecules that are recognized by receptors, which are overexpressed in the target cells.[1−3] It is unlikely, however, that such a strategy proves effective in vivo, as the NCs interact with several biomolecules/structures on-route to the target site. Typically, for simple unmodified NCs, surface adsorption of plasma proteins forms a protein shell that is commonly referred to as the protein "corona",[4−15] a rich protein layer that gives the NC a biological identity that can be very different from its designed synthetic one, in terms of size, curvature, shape, charge, hydrophobicity, surface chemistry, etc. In this view, the protein corona can interfere with active targeting by introducing competing biological signals.[3] A common strategy to limit protein adsorption is by covering the NC surface with moieties such as polyethylene glycol (PEG). However, repeated injections of PEGylated systems promote the splenic synthesis of anti-PEG IgMs that in turn activate the complement system, finally leading to an accelerated blood clearance.[16−18] Furthermore, protein binding to engineered NCs could impair the targeting ability and create a complex protein interface that would result in a new targeting strategy through specific protein−receptor interactions. On the basis of this reasoning, a turning point came up recently: the protein corona that forms upon exposure to biological fluids contains targeting moieties attached thereto.[3,19] Basically, one should design NCs capable of recruiting plasma proteins that are specifically recognized by receptors of the target cells. It has been shown that nanoparticles made of polysorbate-80 (a nonionic surfactant and emulsifier derived from polyethoxylated sorbitan and oleic acid), after administration to mice, become spontaneously covered by apolipoproteins (ApoE is the most enriched) that allow nanoparticles to cross the blood brain barrier.[20,21] Furthermore, Fleischer and Payne[22] demonstrated that the charge nature (i.e., anionic/cationic) of the formed nanoparticle−protein complexes is able to modulate the interaction with target cellular receptors, thus influencing cell binding and uptake. Another recent study by Dittrich et al.[23] has provided further proof of this principle, showing that the cellular uptake

Received: September 25, 2013
Accepted: November 18, 2013
Published: November 18, 2013

  

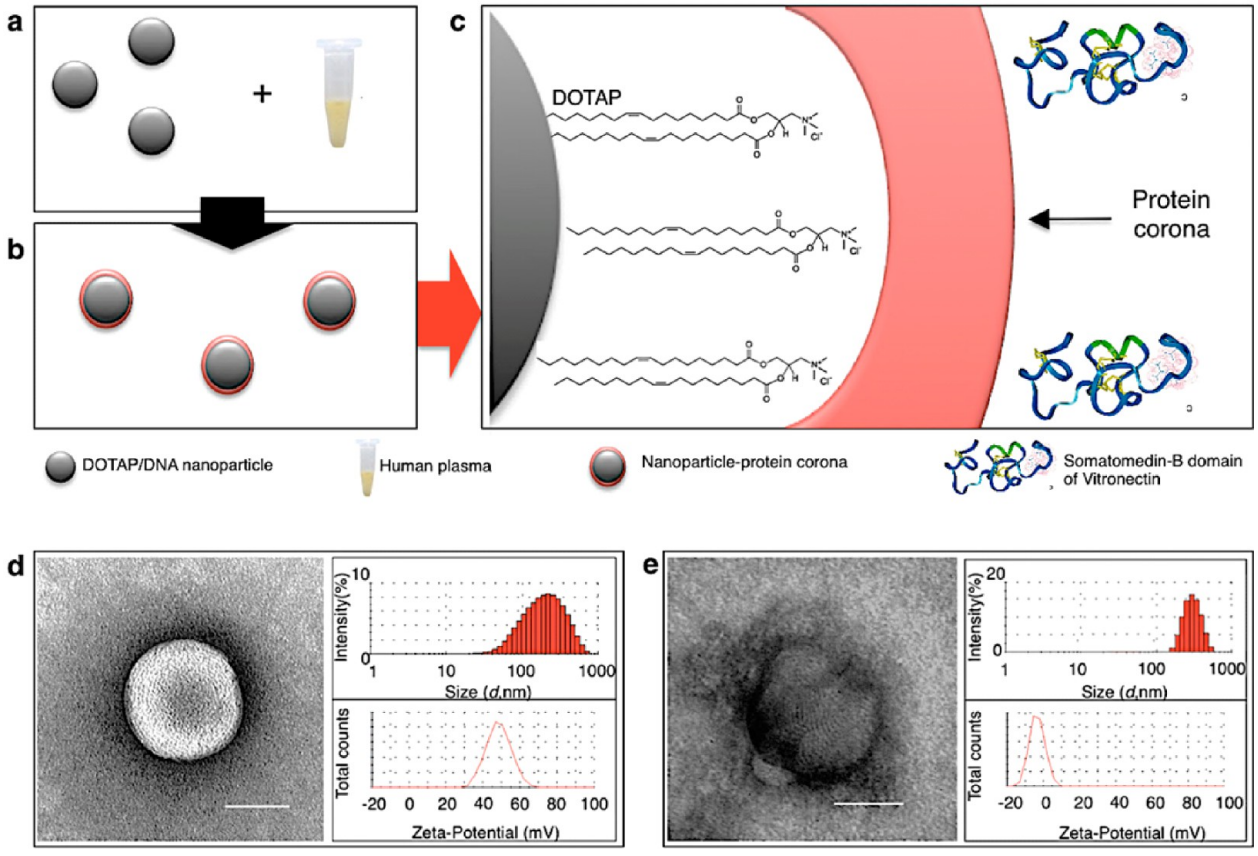


**Figure 1.** Protein corona formation on the nanoparticle surface. (a) When nanoparticles come into contact with human plasma, proteins bind to the surface leading to formation of a rich protein interface called the protein corona (b) that gives to the NP a biological identity distinct from its original synthetic nature. The protein corona of DOTAP lipid nanoparticles (c) is mainly constituted of vitronectin whose Somatomedin-B domain allows us to target cells expressing the vitronectin receptor, i.e., $\alpha_v\beta_3$ integrin. TEM images of DOTAP/DNA lipoplexes (d) and DOTAP/DNA−protein complexes after 1 h incubation with 50% human plasma (e). Scale bars, 200 nm.

of transferrin-coated NCs in Chinese hamster ovary (CHO) cells is mediated by transferrin receptors. Evidently, the "protein corona effect"[3,19] has the potential to lead to a complete renewal of active targeting strategies. To this end, at least two key requisites must be fulfilled: (i) a full quantification of the proteins contained in the corona[10,24−28] and (ii) understanding which of the protein corona components can effectively deliver the NC to a specific location. Thus, it is not surprising that engineering the surface of NCs with plasma proteins with recognized targeting specificity (e.g., transferrin, apolipoproteins, serum albumin, etc.) must be assessed thinking to other biomolecules that shall bind to the surface, as these could obscure their targeting capability.

Following these guidelines, here we will exploit the "protein corona effect" to control the interactions of 1,2-dioleoyl-3-trimethylammonium propane (DOTAP)/DNA cationic liposome/DNA complexes (lipoplexes) with target cells. This lipoplex formulation is widely employed as a model system of gene delivery vectors since it is completely tunable in terms of charge, size, and DNA encapsulation ability.[29] We find that, after exposure to human plasma (HP), DOTAP/DNA lipoplexes become covered with a rich protein corona (Figure 1a,b,c). A quantification of the protein corona composition by nanoliquid chromatography tandem mass spectrometry (NanoLC−MS/MS) coupled to a gene ontology approach to identify the receptors potentially recognized by the corona components allowed us to select the most promising candidates for specific targeting. By combining flow cytometry and two-color fluorescence laser scanning confocal microscopy (LSCM) we prove that vitronectin indeed favors selective uptake of lipoplexes into highly metastatic MDA-MB-435S cells that express high levels of the vitronectin receptor $\alpha_v\beta_3$ integrin.[30] This study provides the proof of concept for exploiting the protein corona effect for targeted nonviral nucleic acid delivery.[3]

## MATERIALS AND METHODS

**Liposome Preparation.** Cationic 1,2-dioleoyl-3-trimethylammonium propane (DOTAP) was purchased from Avanti Polar Lipids (Alabaster, AL) and used without further purification. Briefly, DOTAP was dissolved in chloroform. Chloroform was allowed to evaporate under vacuum for 24 h. Tris-HCl (0.01 M, pH 7.4) buffer was used to hydrate the lipid film (final lipid concentration 1 mg/mL). Then, the liposome dispersion was sonicated by an ultrasound tip sonicator (10 min; 100 W, 20 kHz) and allowed to equilibrate for 24 h at 30 °C.

**Lipoplex Preparation.** To perform laser scanning confocal microscopy, we used Cy3-labeled plasmid DNA (2.7 kbp; 1 mg/mL). Fluorescently labeled DNA was from Mirus Bio Corporation (Madison, WI). Mixing suitable volumes of liposome dispersion and DNA solution, lipoplexes self-assembled. The cationic lipid/DNA charge ratio, $\rho$ (mol/mol), was fixed at $\rho = 2$. At this ratio, lipoplexes usually exhibit maximum transfection efficiency.[31−34] Lipoplexes were incubated with human plasma at different concentrations (0, 2.5, 5, 10, 20, and 50% HP) in a saline buffer (pH 7.4) for one hour. All treatments were performed in a total volume of 1 mL of culture medium.

**Human Plasma Collection.** Human blood was collected from ten healthy volunteers with age comprised between 20 and 40 years who signed an informed consent form. Blood collection was performed in accordance with the guidelines given by the Ethical Committee of the Department of Experimental Medicine at the university of Rome 'Sapienza'. After clotting, blood cells were pelleted by centrifugation (5 min; 1000*g*). Plasma in the supernatant was collected, pooled, aliquoted, and stored at −80 °C by using proper tubes (Protein LoBind tubes). Before use, plasma was thawed at 4 °C and finally warmed at room temperature.

**Size and Zeta-Potential.** The size distribution of cationic liposomes and cationic liposome/DNA complexes (before and after interaction with human plasma) was measured by a NanoZetasizer apparatus (Malvern, UK). More detailed experimental details can be found in refs 31 and 34.

**Transmission Electron Microscopy (TEM).** Samples for TEM were prepared by dispersing a small drop (10 μL) of the suspension on carbon-coated copper grids. The sample was allowed to adsorb on the carbon film for 1 min and after was stained with a 2% uranyl acetate solution for 30 s in the dark at room temperature. Excess of staining was adsorbed with a filter paper, and grids were allowed to air dry for 1 h before observation. Transmission electron micrographics were taken working with an acceleration voltage of 120 keV at a magnification of 30 000× (Libra 120, Zeiss, Germany).

**1D SDS-PAGE.** One-dimensional polyacrylamide gel electrophoresis (1D-PAGE) experiments were performed in triplicate as described elsewhere.[26] To separate plasma proteins we used a 12% polyacrylamide gel, and the gels were stained by Coomassie PhastGel Blue R-350 with mild agitation, following the manufacturer's instructions (GE Healthcare, Milan, Italy).

**NanoLC−MS/MS Analysis.** Identical volumes of HP and DOTAP/DNA lipoplexes (200 μL) were mixed to induce the formation of the protein corona at the nanoparticle surface. One of the major drawbacks is that the nanoparticle−corona composition is temporally modified due to association and dissociation of plasma proteins.[3−13] However, it has been shown that in the majority of reported cases a final equilibrium is reached within 1 h. Thus, in this study, we incubated nanoparticles in human plasma for 1 h. After incubation, the samples were centrifuged to pellet the nanoparticle−protein complexes (10 min; 15000*g*). We washed the pellet three times with the dissolving buffer (250 μL). Then, we transferred the sample into a new tube, and we centrifuged it again. After every single step, tubes were changed to take contamination to a minimum. Subsequently, the pellet was dissolved as elsewhere explained,[24,29] and tryptic digestion was performed by adding 2 μg of trypsin to the solution. After overnight digestion at 37 °C, the reaction was quenched by the addition of trifluoroacetic acid (TFA). Digested samples were desalted using an SPE C18 column (Bond Elut 1CC LRCC18, Varian, Palo Alto, CA, USA). Peptides were eluted from the SPE column with 0.5 mL of ACN:$H_2O$ (50:50, v/v) solution containing 0.05% TFA and were vacuum-dried. Each sample was reconstituted with 0.1% HCOOH solution. Digested samples were stored at −80 °C until nanoLC−MS/MS analysis. For desalting, the peptide mixture was allowed to pass through a solid-phase silica cartridge. Liquid chromatography was performed by a Dionex Ultimate 3000 NanoLC system (Dionex, Sunnyvale, CA, USA). Mass spectrometry detection was done by an LTQ-Orbitrap XL instrument (ThermoFisher Scientific, Bremen, Germany) with a nanospray source, operated in positive ion mode. The LC−MS system was controlled by Xcalibur software (v.2.07, ThermoFisher Scientific). Five technical replicates per sample were performed. Raw data files were submitted to Proteome Discoverer (1.2 version, Thermo Scientific) for database search using Mascot (version 2.3.2 Matrix Science). Data were searched against human entries in the SwissProt protein database (57.15 version, 20 266 sequences), selecting the built-in decoy option. For protein quantitative analysis, the normalization of the spectral countings was made by the Scaffold software. The mean value of the normalized spectral countings (NSCs) obtained in the three experimental replicates for each protein was further normalized to the protein molecular weight (MWNSC) and expressed as the relative protein abundance (RPA). Further experimental details about the experimental procedure can be found elsewhere.[24,29]

**Corona Interactors Meta Analysis.** For each protein in the characterized corona, protein−protein interaction (PPI) data were acquired from MINT,[35] STRING,[36] HPRD,[37] BID,[38] IntAct,[39] and BioGRID[40] databases. Data were then grouped in a nonredundant list of known binary interactions, and gene ontology (GO) details of molecular function and the cellular component were obtained. The complete interactor list was pruned according to GO annotations to obtain a list comprising only genes encoding for proteins with receptorial characteristics and membrane localization. The Novartis Research Foundation Gene Expression Database (GNF) tissue-specific gene expression data set[41] was downloaded from the UCSC Genome Browser. This data set contains genome-wide expression profiles for 79 human tissues and cell lines grouped in eight tissue districts (brain, germ, gland, muscle, nerve, immune, cancer, other). For each gene, replicas were averaged, and only the probe with maximal expression level was taken. As a measure of cumulative probability for a protein to interact with one of its receptors, the expression level of each receptor was summed for every corona protein separately. This measure of cumulative expression was then normalized for the relative abundance in the protein corona. Finally, the normalized expression profile of interactor receptors was compared between each corona protein.

**Cell Culture and Treatments.** HEK 293 and MDA-MB-435S cell lines were purchased from ATCC and cultured following manufacturer's instructions. Cells were maintained at 37 °C in a humidified 5% $CO_2$ atmosphere. At 24 h before the experiment, cotransfection of EGFP-Alpha-V-Integrin and Beta-3-Integrin plasmids[42] was carried out on 70% confluent HEK 293 cells using 0.5 μg of each plasmid and lipofectamine reagent (Invitrogen, Carlsbad, CA) according to the manufacturer's instructions. The day of the experiment the transfected cells were further incubated at 37 °C for 3 h with DOTAP−DNA−Cy3 lipoplexes with or without the adsorbed protein corona (see above).

**Flow Cytometry.** For flow cytometry experiments cells were seeded 24 h before treatment in 6-well plates to reach an 80% confluence at 37 °C. Lipoplexes were given to cells, and incubation lasted 3 h at 37 °C. Subsequently, cells were washed three times in phosphate-buffered saline (PBS). Then, cells were harvested by means of a 0.25% trypsin solution (Invitrogen, Sweden). After 1 min trypsination, cells were centrigufed (5 min; 1200 rpm) and newly dissolved in PBS (500 μL). The uptake of Cy3-labeled lipoplexes was evaluated by 635 nm laser excitation (filter 655−730 nm). For all the tested HP concentrations, $N = 3$ independent experiments were conducted, each in triplicate. A fixed number of 1.5 × 104 cells was acquired for each sample. The MACSQuant analyzer has been used to run samples and MACSQuantify software to analyze data.

**Live Cell Microscopy and Colocalization Assays.** Laser scanning confocal microscopy (LSCM) experiments were performed using a Leica TCS SP5 inverted confocal microscope (Leica Microsystems AG, Wetzlar, Germany), interfaced with an Ar laser for excitation at 488 nm (GFP) and with a He−Ne laser for excitation at 561 nm (Cy3). Petri dishes were inserted into a dedicated chamber (37 °C; 5% $CO_2$) and visualized by a water immersion objective (60 × 1.25). The following collection ranges were adopted: 500−540 nm (GFP) and 570−650 nm (Cy3). Emission was monitored by means of the Acousto-Optical Beam Splitter (AOBS)-based built-in detectors of the confocal microscope. Images were collected in sequential mode to eliminate emission cross talk between the two dyes.

## RESULTS

**Incubation of Lipoplexes with Human Plasma.** DOTAP cationic liposomes were characterized by dynamic light scattering (DLS) and zeta-potential measurements to ensure the formation of monodispersed and positively charged vesicles (Figure S1 in the Supporting Information). Size and Zeta-potential distributions of DOTAP/DNA lipoplexes (cationic lipid/DNA charge ratio, $\rho = 2$) are both shifted with respect to those of the bare DOTAP cationic liposomes

**Table 1. Most Abundant Plasma Proteins Adhering to DOTAP/DNA Lipoplexes After 1 h Incubation with Human Plasma As Identified by Nanoliquid Chromatography Mass Spectrometry[a]**

| identified protein | description | RPA (10% HP) | RPA (50% HP) |
|---|---|---|---|
| P04004\|VTNC_HUMAN | Vitronectin | 31.3 | 32.2 |
| P02768\|ALBU_HUMAN | Serum albumin | 17.3 | 17.0 |
| P02652\|APOA2_HUMAN | Apolipoprotein A-II | 9.4 | 9.8 |
| P01024\|CO3_HUMAN | Complement C3 | 7.5 | 7.8 |
| P02656\|APOC3_HUMAN | Apolipoprotein C-III | 7 | 6.5 |
| P02655\|APOC2_HUMAN | Apolipoprotein C-II | 6.6 | 6.9 |
| Q14520\|HABP2_HUMAN | Hyaluronan-binding protein 2 | 4.7 | 4.5 |
| P02675\|FIBB_HUMAN | Fibrinogen beta chain | 3.8 | 3.5 |
| P10909\|CLUS_HUMAN | Clusterin | 3.1 | 3.3 |
| P04114\|APOB_HUMAN | Apolipoprotein B-100 | 2.9 | 3.0 |
| P02675\|FIBB_HUMAN | Fibrinogen gamma chain | 3.1 | 2.8 |
| P27169\|PON1_HUMAN | Serum paraoxonase/arylesterase | 1.2 | 1.0 |
| P19827\|ITIH1_HUMAN | Interalpha-trypsin inhibitor heavy chain H1 | 0.6 | 0.5 |
| P02760\|AMBP_HUMAN | Protein AMBP | 0.6 | 0.5 |
| P04003\|C4BPA_HUMAN | C4b-binding protein alpha chain | 0.4 | 0.4 |
| P00734\|THRB_HUMAN | Prothrombin | 0.3 | 0.2 |
| P07225\|PROS_HUMAN | Vitamin K-dependent protein S | 0.2 | 0.1 |

[a]According to ref 10 the contribution of proteins can be evaluated by calculating the relative protein abundance (RPA). A RPA threshold of 3% was chosen for corona expression meta-analysis (indicated by gray shades).

(Figure S1 in the Supporting Information). Size enlargement and reduction in zeta-potential are typical occurrences in lipoplex formation.[29] Upon formation of liposome/DNA complexes, DNA and lipids rearrange into multilamellar particles with DNA embedded within alternating lipid layers as revealed by transmission electron microscopy (TEM) (Figure 1d).[29] DOTAP/DNA lipoplexes were incubated with human plasma for 1 h, and the resulting lipoplex−protein complexes were separated from excess plasma to eliminate the unbound proteins (see sample preparation in the Materials and Methods section). Formation of the protein corona is schematically shown in Figure 1a−c. Protein binding was demonstrated by one-dimensional sodium dodecyl sulfate-polyacrylamide gel electrophoresis (1D SDS-PAGE). In 1D SDS-PAGE experiments, DOTAP/DNA lipoplexes were incubated in plasma concentrations from 2.5% to 80% (Figure S2A in the Supporting Information). The identity of the main protein bands does not change with increasing plasma concentration, while the intensity of bands increases in a monotonous fashion (i.e., more proteins of the same type bind at higher concentrations) (Figure S2B in the Supporting Information). Formation of the protein corona around lipoplexes is confirmed by the direct visualization of the NP−protein−corona complex through TEM analysis and leads to a negative zeta-potential and a significantly larger particle hydrodynamic diameter (Figure 1e). Even though monomers are largely predominant, we also observe a minor fraction of dimers and trimers (Figure S3 in the Supporting Information). Next, we used NanoLC−MS/MS to determine the composition of protein corona quantitatively. Table 1 contains the relative protein abundance of the plasma proteins adhering to DOTAP/DNA lipoplexes after 1 h incubation (10% and 50% HP). Despite the complexity of the system, the proteins extracted from the lipoplex surfaces are highly reproducible. NanoLC−MS/MS confirms our above suggestion based on 1D SDS-PAGE results that the protein corona composition does not change with increasing plasma concentration. Thus, hereafter we will restrict our analysis to the biologically relevant 50% HP condition, in line with previous reports.[3−13] We found that vitronectin and serum albumin are the most abundant proteins associated with the surface of DOTAP/DNA lipoplexes. The sum of the RPA of vitronectin plus that of serum albumin is about 50%.

**Corona Interactor Meta Analysis.** To rationalize the identification of the receptors potentially associated with the protein corona components, a detailed meta analysis has been performed (see Materials and Methods section). For the ten corona proteins previously selected, a complete list of receptors was obtained using protein−protein interaction (PPI) data (Figure 2).[35−41] The list was pruned according to GO annotations to comprise only those genes that encode for proteins with both a receptor activity and localized on the outer leaflet of the plasma membrane. For each gene, replicas were averaged, and only the probe with maximal expression level was taken. As a measure of cumulative probability for a protein to interact with one of its receptors, the expression level of each receptor was summed for every corona protein separately. This measure of cumulative expression was finally normalized for the RPA of the most significant proteins found in the protein corona. Since results reported in Figures 2 and 3 depend on the quantitative composition of the protein corona (Table 1), we emphasize that different corona compositions will result in distinct cumulative expression of receptors associated with the corona of nanoparticle−protein complexes.

Comparing the expression profile of all the corona proteins the prominent role of vitronectin clearly appears since its receptor counterparts are generally expressed in each tissue district analyzed (Figure 3). Vitronectin contains the Arg-Gly-Asp (RGD) motif in the Somatomedin B domain (20−63 region) that is specifically recognized by $\alpha_v\beta_3$ integrins, which are overexpressed on many solid tumors and in tumor neovasculature. To exploit the protein corona effect in vitro highly metastatic MDA-MB-435S cells that express high levels of the vitronectin receptor $\alpha_v\beta_3$ integrin[30] were used as an experimental model, while Human Embryonic Kidney (HEK 293) that express remarkably low levels of the same receptor[30] were used as a reference. However, it should be underlined that a real tumor/cancer does contain a variety of cell types, and

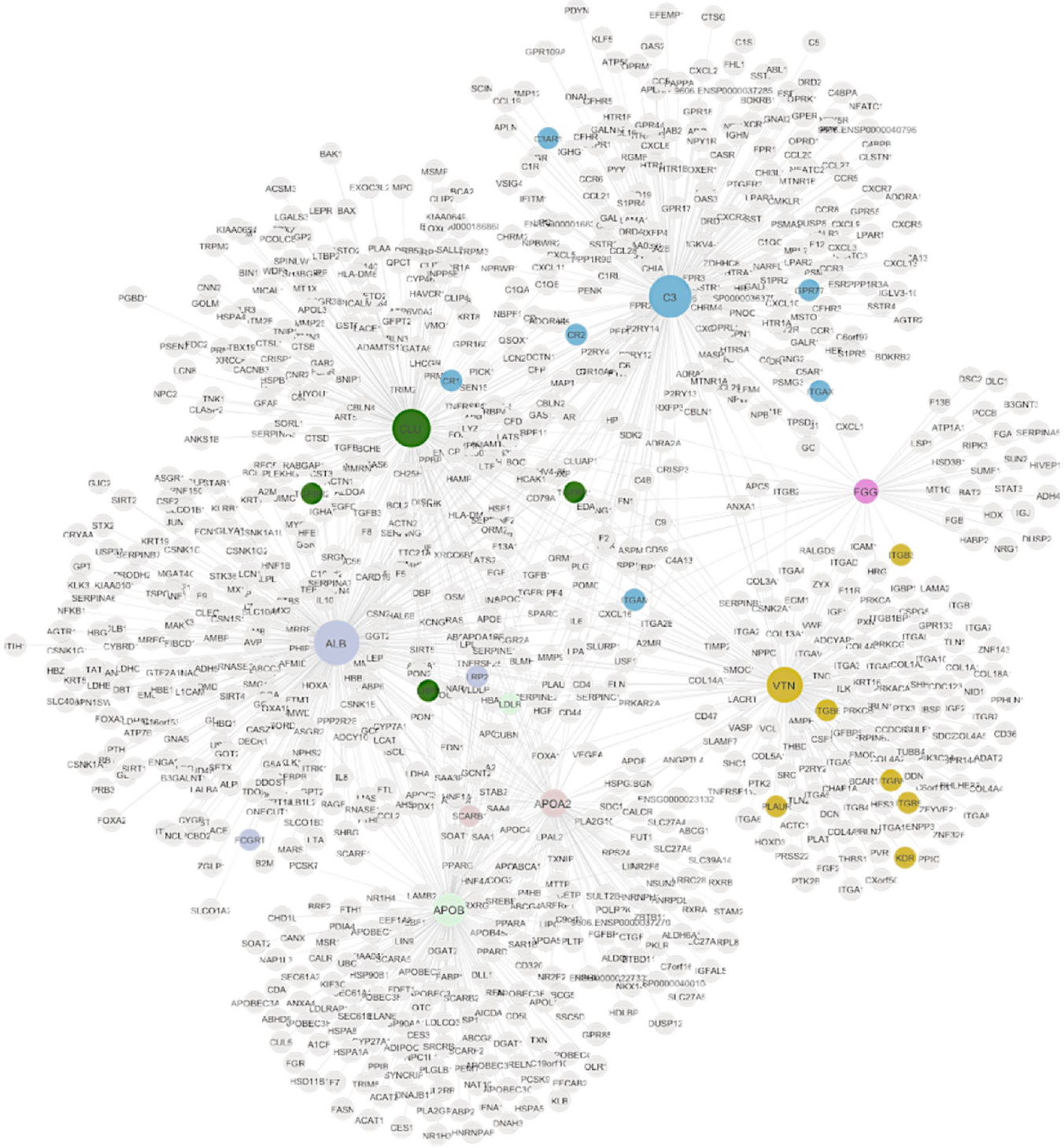


**Figure 2.** Corona protein interaction network. Protein−protein interaction data were obtained and grouped from different databases. Receptorial interactors are colored relative to the protein they interact with.

efficient therapies might need to target most of these cell types notably including cancer stem cells. Because expression of $\alpha$(v) integrins on distinct cell types contributes to cancer growth, targeting of $\alpha$(v) integrin antagonists also has the potential to disrupt multiple aspects of disease progression. For instance, given their relevant role in angiogenesis, blocking the $\alpha$(v) integrin could be a good strategy to produce an antiangiogenic effect.[43] It has been recently shown that $\alpha$(v) integrins also play an important role in maintaining the cancer stem/progenitor pool.[44] In addition, in preclinical models of prostate cancer it has been demonstrated that blocking $\alpha$(v) integrins can inhibit the de novo formation and progression of bone metastases.[45]

**Cellular Uptake of Lipoplexes Is Enhanced by the Protein Corona.** To test the "protein corona effect" for targeted delivery, we have compared the cellular uptake of DOTAP/DNA lipoplexes and DOTAP/DNA−protein complexes in $\alpha_v\beta_3$ receptor-positive MDA-MB-435S and $\alpha_v\beta_3$ receptor-negative HEK 293 cells using flow cytometry.

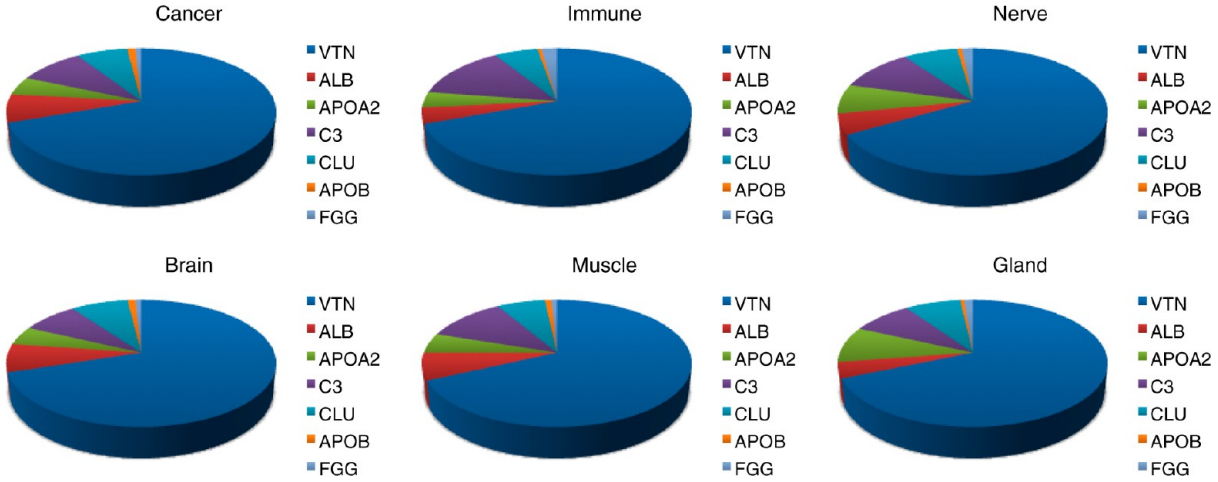


**Figure 3.** Cumulative expression of receptors associated with the lipoplex corona. VTN: Vitronectin; ALB: Serum albumin; APOA2: Apolipoprotein A-II; C3: Complement C3; CLU: Clusterin; APOB: Apolipoprotein B-100; FGG: Fibrinogen beta chain.

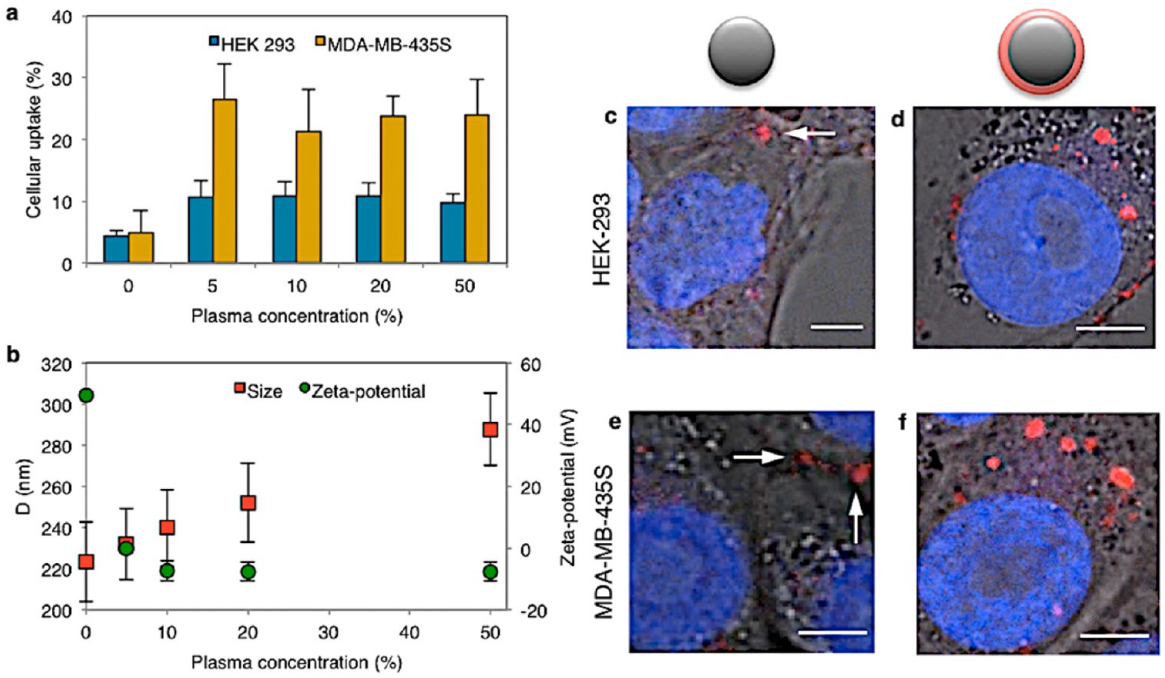


**Figure 4.** Enhancement of nanoparticle cell uptake in the presence of protein corona. (a) Cellular uptake of DOTAP/DNA protein complexes after interaction with increasing concentration of human plasma in HEK 293 and MDA-MB-435S cell lines. (b) Size and zeta-potential of DOTAP/DNA lipoplex–protein complexes. Confocal images of HEK 293 and MDA-MB-435S cells treated with DOTAP/DNA lipoplexes (c,d) and DOTAP/DNA lipoplex–protein complexes (e,f). Cell nucleus stained with DAPI. Scale bars, 1 $\mu$m.

DOTAP/DNA lipoplexes exhibit very similar cellular uptake in both the receptor-positive and receptor-negative cells (Figure 4A). This is most likely to indicate that cellular uptake of the bare lipoplexes is a nonspecific process.[46,47] This is in line with recent reports, which showed that DOTAP-containing lipoplexes are taken up by cells mainly through fluid-phase macropinocytosis.[46,47] Given the larger uptake of cationic complexes compared to their anionic counterparts,[48] the negative surface charge of DOTAP/DNA–protein assemblies (Figure 4B) would be expected to make the interaction with the negatively charged proteoglycans at the plasma membrane less favorable. Notably, on the opposite, Figure 4a shows that the cellular uptake of DOTAP/DNA–protein complexes is enhanced by roughly a factor 5 in receptor-positive MDA-MB-435S cells with respect to the bare lipoplexes. A lower but appreciable increase (about 2-fold) was found in receptor-negative HEK 293 cells. As above-mentioned, in a real tumor/cancer different cell types exist with potentially a different coverage of negatively charged proteoglycans. Thus, the role of the protein corona on the aspecific cellular uptake of nanoparticles is expected to depend both on tumor type and on target cells in the tumor.

We next examined the intracellular distribution of DOTAP/DNA complexes both in the presence and in the absence of the protein corona. Confocal images show that DOTAP/DNA–protein complexes are more abundantly distributed throughout the cytosol of both MDA-MB-435S and HEK 293 cells (Figure 4c,d,e,f).

**Uptake of Lipoplexes Occurs by Specific Corona–Receptor Interaction.** To determine if the vitronectin

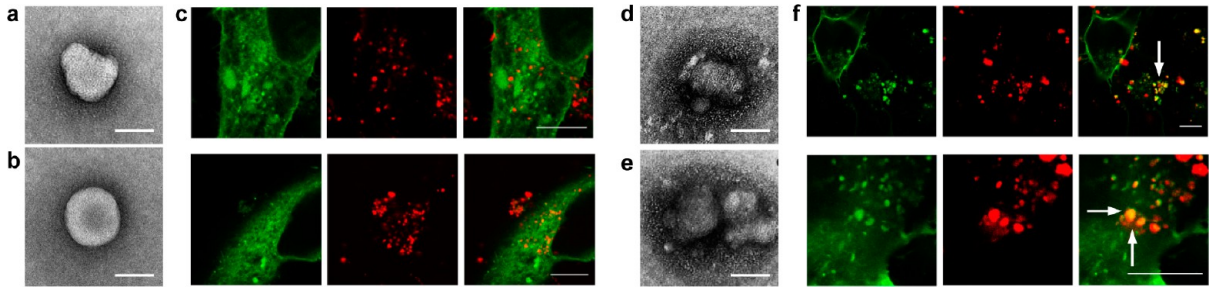


**Figure 5.** Internalization mechanism of nanoparticle−protein complexes. (a,b) TEM images of typical DOTAP/DNA lipoplexes. Scale bars, 200 nm. (c) Confocal images of HEK 293 cells expressing GFP-conjugated $\alpha_v\beta_3$ integrin treated with fluorescently labeled DOTAP/DNA lipoplexes (red). No clear evidence of fluorescence signal colocalization was found. When HEK 293 cells expressing GFP-conjugated $\alpha_v\beta_3$ integrin were treated with DOTAP/DNA−protein complexes (d,e, scale bars 200 nm), large colocalization of green and red fluorescence signals (f) reveals that DOTAP/DNA−protein complexes are mainly found within vitronectin receptor $\alpha_v\beta_3$-positive vesicles (indicated by arrows).

receptor (i.e., $\alpha_v\beta_3$) is truly responsible for the protein-dependent binding of DOTAP−DNA−protein complexes, we monitored the localization of Cy-3-labeled lipoplexes (red) and GFP-labeled vitronectin receptors (green) in live cells using LSCM. As MDA-MB-435S expresses high levels of $\alpha_v\beta_3$ receptor, a distinction between GFP-conjugated and untagged (i.e., constitutionally expressed) integrins would be ineffective. On the contrary, in HEK 293 cells expressing GFP-conjugated integrins (GFP−$\alpha_v$ integrin coexpressed with untagged $\beta_3$ integrin, as described by others;[42] see also Methods section), if our assumptions are correct, we expect colocalization of red and green signals giving rise to visible yellow/orange punctuate structures. Figure 5 shows that that fluorescently labeled DOTAP/DNA lipoplexes exhibit minimal, if any, colocalization with GFP-conjugated integrin. Notably, red-labeled DOTAP/DNA−protein complexes largely colocalized with a green signal revealing that, in the presence of the protein corona, complexes strongly colocalize with vitronectin receptor $\alpha_v\beta_3$-positive vesicles. As a control, we preincubated HEK 293 cells with free RGD peptide for 1 h. Then, fluorescently labeled DOTAP/DNA−protein complexes were given to cells. In that case, complexes (red) did not show clear colocalization with GFP-conjugated integrin (green) (Figure S4 in Supporting Information).

## DISCUSSION AND CONCLUSIONS

Nanotechnology has held great promise for therapy and medicine giving rise to the emerging field of nanomedicine. The toughest challenge arises when nanomaterials come into contact with biological fluids, such as HP. Here biomolecules, especially proteins, bind to the surface of the nanoparticle, forming a cloud of aggregated proteins known as a "protein corona".[3] The nonspecific adsorption and the resulting corona have been widely viewed as negative side effects. More recently, it has been recognized that the protein corona mediates the interaction of the nanomaterial with biomolecules, membranes, and physical barriers. The debate has prompted the suggestion to factor its unique properties into nanomaterial design instead of trying to avoid its existence. What is needed to exploit protein coronas for specific cell targeting? First, we need to characterize the biological identity of the nanoparticle (surface charge, size, and quantitative protein corona composition). Then, we have to understand how it influences the physiological response. In the present study, we used a common gene delivery system made of the cationic lipid DOTAP and DNA. DOTAP/DNA lipoplexes ($\rho$ = 2) were found to be positively charged multilamellar particles with DNA embedded within alternating lipid layers (Figure 1). Since blood is the first physiological environment nanoparticle "seen" after intravenous administration, we investigated the interaction between DOTAP/DNA complexes and HP, the acellular portion of human blood, which is known to contain over 1000 proteins. Exposure of DOTAP/DNA complexes to HP resulted in the formation of a protein corona as demonstrated by 1D SDS-PAGE and by the direct visualization of the NP−protein−corona complex through TEM analysis (Figure 1e). In the presence of the corona, complexes were negatively charged and larger in size than bare lipoplexes. The identity and quantity of the adsorbed proteins determines the array of possible biological interactions along with their strengths. Due to its immense complexity, the protein corona has been challenging to characterize. Identification and quantification of individual proteins within the corona is generally performed after isolation of the adsorbed protein from the nanomaterial surface. Among such techniques, nanoLC−MS/MS has been applied for simultaneous identification and quantification of the protein corona with higher throughput and great accuracy.[24−28] NanoLC−MS/MS allowed us to determine the composition of the protein corona of DOTAP/DNA−HP complexes quantitatively (Table 1). Coupling NanoLC−MS/MS and GO we identified vitronectin as the most promising corona component for active targeting (Figure 3). Vitronectin is recognized by $\alpha_v\beta_3$ integrins, also known as the vitronectin receptor, which are overexpressed on many solid tumors and in tumor neovasculature. Thus, we exploited the protein corona to target highly metastatic MDA-MB-435S cells that express high levels of the vitronectin receptor $\alpha_v\beta_3$ integrin,[30] while Human Embryonic Kidney (HEK 293) cells that express remarkably low levels of the same receptor[30] were used as a reference. Notably, the cellular uptake of DOTAP/DNA−protein complexes was enhanced by a factor of 5 in receptor-positive MDA-MB-435S cells with respect to the bare lipoplexes. At this level, it is tough to separate out and quantify uptake via targeted receptors from that due to physicochemical nonspecific adhesion of the nanocarrier to the cell surface. However, based on our NanoLC−MS/MS quantitative analysis and meta analysis screening, we were tempted to ascribe to vitronectin the responsibility for the increased uptake in $\alpha_v\beta_3$ receptor-positive MDA-MB-435S cells. This is most likely to indicate binding caused by a specific corona−receptor interaction. Clearly, uptake levels are not necessarily related to receptor-mediated internalization. Under this hypothesis, it is unclear how to explain the 2-fold increase in cellular uptake observed in $\alpha_v\beta_3$-receptor negative HEK 293. However, we cannot exclude

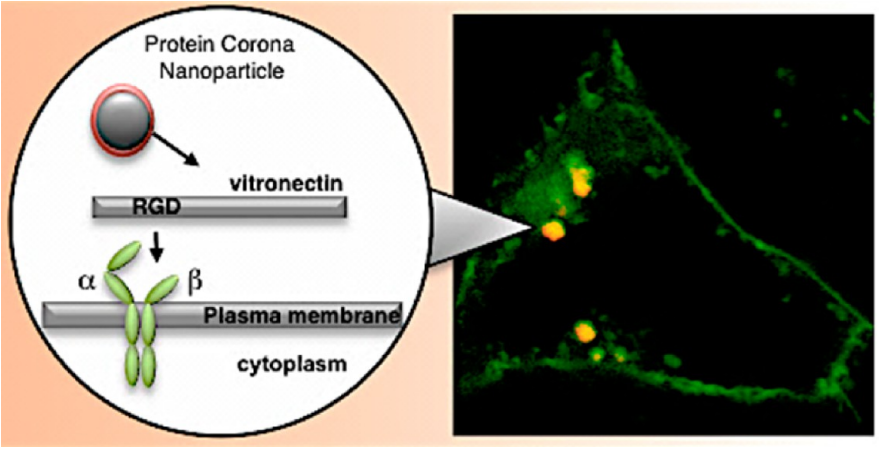


**Figure 6.** Receptor-mediated internalization of nanoparticles. (left) Cartoon describing the cell uptake of nanoparticles when a biomolecule corona adsorbs on the surface. After exposure to human plasma, nanoparticles become covered with a rich protein corona. Quantitative determination of the protein corona composition allows us to identify the most promising protein corona component for active targeting. (right) When exposed to HP, DOTAP lipid nanoparticles (red) are covered by vitronectin that contains the Arg-Gly-Asp (RGD) that is specifically recognized by $\alpha_v\beta_3$ integrins (green).

that (*i*) receptors other than $\alpha_v\beta_3$ can interact with the corona proteins or (*ii*) the protein corona as a whole can modify the interaction with target cells by altering some other nanoparticle properties such as, for instance, the size and/or the charge. To test the functionality of the corona in mediating a specific surface receptor, a proof more robust than increase in cellular uptake was needed. To this end, two-color LSCM was used. LSCM results proved that the bare lipoplexes do not bind to vitronectin receptors before being internalized (Figure 5c). Notably, we could demonstrate that, in the presence of protein corona, complexes strongly colocalize with vitronectin receptor $\alpha_v\beta_3$-positive vesicles (Figure 5f). These results suggest a major contribution of receptors when a protein corona adsorbs on the surface (Figure 6). This integrated proteomics, bioinformatics, and nanotechnology strategy demonstrates that protein corona identification can be used to deliver therapeutics to target cells. Further study may provide important insights into how the protein corona can be exploited for a practical application in vivo.

## ■ ASSOCIATED CONTENT

### Supporting Information

Figure S1. Size and Zeta-Potential distributions of DOTAP cationic liposomes, DOTAP/DNA lipoplexes, and DOTAP/DNA lipoplex−protein complexes.

Figure S2. One-dimensional SDS-PAGE gel of human plasma proteins obtained from DOTAP/DNA lipoplex−protein complexes following incubation at different plasma concentrations.

Figure S3. TEM images of lipoplex−protein complexes after 1 h incubation with 50% human plasma.

Figure S4. Confocal images of HEK 293 cells expressing GFP-conjugated $\alpha v\beta 3$ integrin (green) treated with DOTAP/DNA−protein complexes (red) after 1 h incubation with RGD peptide. This material is available free of charge via the Internet at http://pubs.acs.org.

## ■ AUTHOR INFORMATION

### Corresponding Author

*E-mail: giulio.caracciolo@uniroma1.it.

### Author Contributions

#Equal contribution. G.C. wrote the article. All authors have given approval to the final version of the manuscript.

### Notes

The authors declare no competing financial interest.

## ■ ACKNOWLEDGMENTS

This work was partially supported by the Italian Minister for University and Research (MIUR) (Futuro in Ricerca 2008, grant no. RBFR08TLPO; PRIN 2009, prot. 2009ACFPN9). GC, DP, ALC, CC. and AL acknowledge support by the Istituto Italiano di Tecnologia, Center for Life Nano Science@Sapienza.

## ■ REFERENCES

(1) Béduneaua, A.; Saulniera, P.; Benoit, J.-P. *Biomaterials* **2007**, *28*, 4947−4967.
(2) Choi, C. H. J.; Alabi, C. A.; Webster, P.; Davis, M. E. *Proc. Natl. Acad. Sci. U.S.A.* **2010**, *107*, 1235−1240.
(3) Mahon, E.; Salvati, A.; Baldelli Bombelli, F.; Lynch, I.; Dawson, K. A. *J. Controlled Release* **2012**, *161*, 164−174.
(4) Cedervall, T.; Lynch, I.; Foy, M.; Berggard, T.; Donnelly, S. C.; Cagney, G.; Linse, S.; Dawson, K. A. *Angew. Chem., Int. Ed.* **2007**, *46*, 5754−5756.
(5) Lynch, I.; Cedervall, T.; Lundqvist, M.; Cabaleiro-Lago, C.; Linse, S.; Dawson, K. A. *Adv. Colloid Interface Sci.* **2007**, *134*−*135*, 167−174.
(6) Lundqvist, M.; Stigler, J.; Cedervall, T.; Elia, G.; Lynch, I.; Dawson, K. A. *Proc. Natl. Acad. Sci. U.S.A.* **2008**, *105*, 14265−14270.
(7) Lynch, I.; Dawson, K. A. *Nano Today* **2008**, *3*, 40−47.
(8) Walczyk, D.; Baldelli Bombelli, F.; Monopoli, M. P.; Lynch, I.; Dawson, K. A. *J. Am. Chem. Soc.* **2010**, *132*, 5761−5768.
(9) Lesniak, A.; Campbell, A.; Monopoli, M. P.; Lynch, I.; Salvati, A.; Dawson, K. A. *Biomaterials* **2010**, *31*, 9511−9518.
(10) Monopoli, M. P.; Walczyk, D.; Campbell, A.; Elia, G.; Lynch, I.; Baldelli Bombelli, F.; Dawson, K. A. *J. Am. Chem. Soc.* **2011**, *133*, 2525−2534.
(11) Monopoli, M. P.; Baldelli Bombelli, F.; Dawson, K. A. *Nat. Nanotechnol.* **2011**, *6*, 11−12.
(12) Lundqvist, M.; Stigler, J.; Cedervall, T.; Berggård, T.; Flanagan, M. B.; Lynch, I.; Elia, G.; Dawson, K. A. *ACS Nano* **2011**, *5*, 7503−7509.
(13) Salvati, A.; Ãberg, C.; dos Santos, T.; Varela, J.; Pinto, P.; Lynch, I.; Dawson, K. A. *Nanomedicine* **2011**, *7*, 818−826.

(14) Walkey, C. D.; Olsen, J. B.; Guo, H.; Emili, A.; Chan, W. C. *J. Am. Chem. Soc.* **2012**, *134*, 2139−2147.
(15) Walkey, C. D.; Chan, W. C. W. *Chem. Soc. Rev.* **2012**, *41*, 2780−2799.
(16) Ishida, T.; Harada, M.; Wang, X .Y.; Ichihara, M.; Irimura, K.; Kiwada, H. *J. Controlled Release* **2008**, *105*, 305−317.
(17) Zhao, Y.; Wang, C.; Wang, L.; Yang, Q.; Tang, W.; She, Z.; Deng, Y. *Eur. J. Pharm. Biopharm.* **2012**, *81*, 506−513.
(18) Zhao, Y.; Wang, L.; Yan, M.; Ma, Y.; Zang, G.; She, Z.; Deng, Y. *Int. J. Nanomed.* **2012**, *7*, 2891−2900.
(19) Caracciolo, G. *Bioinspired, Biomimetic Nanobiomater.* **2013**, *2*, 54−57.
(20) Kreuter, J.; Shamenkov, D.; Petrov, V.; Ramge, P.; Cychutek, K.; Koch-Brandt, C.; Alyautdin, R. *J. Drug Targeting* **2002**, *10*, 317−325.
(21) Kreuter, J. *J. Nanosci. Nanotechnol.* **2004**, *4*, 484−488.
(22) Fleischer, C. C.; Payne, C. K. *J. Phys. Chem. B* **2012**, *116*, 8901−8907.
(23) Dittrich, C.; Burckhardt, C. J.; Danuser, G. *Biomaterials* **2012**, *33*, 2746−2753.
(24) Capriotti, A. L.; Caracciolo, G.; Cavaliere, C.; Crescenzi, C.; Pozzi, D.; Laganà, A. *Anal. Bioanal. Chem.* **2011**, *401*, 1195−1202.
(25) Capriotti, A. L.; Caracciolo, G.; Caruso, G.; Foglia, P.; Pozzi, D.; Samperi, R.; Laganà, A. *Anal. Biochem.* **2011**, *419*, 180−189.
(26) Capriotti, A. L.; Caracciolo, G.; Caruso, G.; Foglia, P.; Pozzi, D.; Samperi, R.; Laganà, A. *Proteomics* **2011**, *11*, 3349−3358.
(27) Capriotti, A. L.; Caracciolo, G.; Cavaliere, C.; Foglia, P.; Pozzi, D.; Samperi, R.; Laganà, A. *J. Proteomics* **2012**, *75*, 1924−1932.
(28) Capriotti, A. L.; Caracciolo, G.; Caruso, G.; Cavaliere, C.; Pozzi, D.; Samperi, R.; Laganà, A. *Anal. Bioanal. Chem.* **2013**, *405*, 635−645.
(29) Caracciolo, G.; Pozzi, D.; Capriotti, A. L.; Marianecci, C.; Carafa, M.; Marchini, C.; Montani, M.; Amici, A.; Amenitsch, H.; Digman, M. A.; Gratton, E.; Sanchez, S. S.; Laganà, A. *J. Med. Chem.* **2011**, *54*, 4160−4171.
(30) Taherian, A.; Li, X.; Liu, Y.; Haas, T. A. *BMC Cancer* **2011**, *11*, 293.
(31) Pozzi, D.; Marchini, C.; Cardarelli, F.; Bifone, A.; Garulli, C.; Caracciolo, G. *Biochim. Biophys. Acta, Biomembr.* **2012**, *1818*, 2335−2343.
(32) Caracciolo, G.; Amenitsch, H. *Eur. Biophys. J.* **2012**, *41*, 815−829.
(33) Coppola, C.; Estrada, L. C.; Digman, M. A.; Gratton, E.; Caracciolo, G. *Soft Matter* **2012**, *8*, 7919−7927.
(34) Coppola, C.; Cardarelli, F.; Pozzi, D.; Estrada, L. C.; Digman, M. A.; Gratton, E.; Bifone, A.; Caracciolo, G. *Ther. Delivery* **2013**, *4*, 191−202.
(35) Licata, L.; Briganti, L.; Peluso, D.; Perfetto, L.; Iannuccelli, M.; Galeota, E.; Sacco, F.; Palma, A.; Nardozza, A. P.; Santonico, E.; Castagnoli, L.; Cesareni, G. *Nucleic Acids Res.* **2012**, *40*, D857−D861.
(36) Szklarczyk, D.; Franceschini, A.; Kuhn, M.; Simonovic, M.; Roth, A.; Minguez, P.; Doerks, T.; Stark, M.; Muller, J.; Bork, P.; et al. *Nucleic Acids Res.* **2011**, No. 39, D561−D568.
(37) Prasad, T. S. K.; Kandasamy, K.; Pandey, A. *Methods Mol. Biol.* **2009**, *577*, 67−79.
(38) Bader, G. D.; Betel, D.; Hogue, C. W. V. *Nucleic Acids Res.* **2003**, *31*, 248−250.
(39) Kerrien, S.; Aranda, B.; Breuza, L.; Bridge, A.; Broackes-Carter, F.; Chen, C.; Duesbury, M.; Dumousseau, M.; Feuermann, M.; Hinz, U.; et al. *Nucleic Acids Res.* **2012**, *40*, D841−D846.
(40) Winter, A. G.; Wildenhain, J.; Tyers, M. *Bioinformatics* **2011**, *27*, 1043−1044.
(41) Su, A. I.; Wiltshire, T.; Batalov, S.; Lapp, H.; Ching, K. A.; Block, D.; Zhang, J.; Soden, R.; Hayakawa, M.; Kreiman, G.; et al. *Proc. Natl. Acad. Sci. U.S.A.* **2004**, *101*, 6062−6067.
(42) Hu, K.; Ji, L.; Applegate, K. T.; Danuser, G.; Waterman-Storer, C. M. *Science* **2007**, *315*, 111−115.
(43) Foubert, P.; Varner, J. A. *Methods Mol. Biol.* **2012**, *757*, 471−86.
(44) van den Hoogen, C.; van der Horst, G.; Cheung, H.; Buijs, J. T.; Pelger, R. C.; van der Pluijm, G. *Am. J. Pathol.* **2011**, *179*, 2559−68.
(45) van der Horst, G.; van den Hoogen, C.; Buijs, J. T.; Cheung, H.; Bloys, H.; Pelger, R. C.; Lorenzon, G.; Heckmann, B.; Feyen, J.; Pujuguet, P.; Blanque, R.; Clément-Lacroix, P.; van der Pluijm, G. *Neoplasia* **2011**, *13*, 516−25.
(46) Cardarelli, F.; Pozzi, D.; Bifone, A.; Marchini, C.; Caracciolo, G. *Mol. Pharmaceutics* **2012**, *9*, 334−340.
(47) Zhang, X.-X.; Allen, P. G.; Grinstaff, M. *Mol. Pharmaceutics* **2011**, *8*, 758−766.
(48) Felgner, P. L.; Gadek, T. R.; Holm, M.; Roman, R.; Chan, H. W.; Wenz, M.; Northrop, J. P.; Ringold, G. M.; Danielsen, M. *Proc. Natl. Acad. Sci. U.S.A.* **1987**, *84*, 7413−7417.